IJC
International Journal of Cancer

Transforming growth factor beta-induced, an extracellular matrix interacting protein, enhances glycolysis and promotes pancreatic cancer cell migration

Brunella Costanza[1], Gilles Rademaker[1], Assia Tiamiou[1], Pascal De Tullio[2], Justine Leenders[2], Arnaud Blomme[3], Justine Bellier[1], Elettra Bianchi[4], Andrei Turtoi[5], Philippe Delvenne[4,6], Akeila Bellahcène[1], Olivier Peulen[1†] and Vincent Castronovo[1†]

[1]Metastasis Research Laboratory, GIGA Cancer, University of Liège, Liège, Belgium
[2]Center for Interdisciplinary Research on Medicines, Metabolomics Group, University of Liège, Liège, Belgium
[3]Cancer Research UK Beatson Institute, Glasgow, United Kingdom
[4]Department of Pathology, University Hospital (CHU), University of Liège, Liège, Belgium
[5]Tumor Microenvironment and Resistance to Treatment Laboratory, Institut de Recherche en Cancérologie de Montpellier, Montpellier, France
[6]Laboratory of Experimental Pathology, GIGA Cancer, University of Liège, Liège, Belgium

Pancreatic ductal adenocarcinoma (PDAC) remains a deadly malignancy with no efficient therapy available up-to-date. Glycolysis is the main provider of energetic substrates to sustain cancer dissemination of PDAC. Accordingly, altering the glycolytic pathway is foreseen as a sound approach to trigger pancreatic cancer regression. Here, we show for the first time that high transforming growth factor beta-induced (TGFBI) expression in PDAC patients is associated with a poor outcome. We demonstrate that, although usually secreted by stromal cells, PDAC cells synthesize and secrete TGFBI in quantity correlated with their migratory capacity. Mechanistically, we show that TGFBI activates focal adhesion kinase signaling pathway through its binding to integrin αVβ5, leading to a significant enhancement of glycolysis and to the acquisition of an invasive phenotype. Finally, we show that TGFBI silencing significantly inhibits PDAC tumor development in a chick chorioallantoic membrane assay model. Our study highlights TGFBI as an oncogenic extracellular matrix interacting protein that bears the potential to serve as a target for new anti-PDAC therapeutic strategies.

Introduction

Pancreatic ductal adenocarcinoma (PDAC) is one of the deadliest pathologies worldwide, with a 5-year overall survival limited to 8%,[1] and is projected to become the second leading cause of cancer-related death by 2030.[2] PDAC remains silent for long periods of time before inducing clinical symptoms, which are usually unspecific. As a consequence, it is diagnosed at a late stage, when metastatic dissemination has often occurred.[3] Despite great advances in clinical oncology, there are still no sensitive biomarkers for early diagnosis as well as no validated molecular targets for therapies.[4] Therapeutic options remain very limited and are based on classical cytotoxic compounds, often poorly tolerated and with modest outcome benefits. Thus, there is an urgent need to identify, to validate and to clinically test new molecular therapeutic targets. At cellular and molecular levels, PDAC is characterized by hypovascularization,[5] complex landscape of genomic mutations,[6] altered metabolism[7] and exuberant stromal reaction (desmoplasia).[8] The latter consists in the deposition of extracellular matrix (ECM) components around cancer cells. ECM is a strong regulator of tumor growth and dissemination. It is composed of specialized secreted proteins and proteoglycans that provide support to the resident cells. Modification in ECM composition and/or cell–matrix interaction has a relevant impact on several processes, including cell survival, proliferation, differentiation, migration, cancer cell invasion and resistance to therapies.[9,10] In this scenario, integrin family members are the major cellular receptors for ECM proteins that play essential role in all the steps of cell migration.[11] Integrin–ECM protein interactions occur mainly through the binding at Arg-Gly-Asp (RGD) motif. TGFBI (transforming growth factor beta-induced) is a secreted 68 kDa protein composed of an RGD motif in its C-terminal region. Secreted

Key words: pancreas, TGFBI, integrin, extracellular matrix, glycolysis
Additional Supporting Information may be found in the online version of this article.
Conflicts of interest: Authors have no conflict of interest to disclose.
†O.P. and V.C. contributed equally to this work and shared last authorship
Grant sponsor: Fonds De La Recherche Scientifique - FNRS; **Grant sponsor:** Fonds Léon Fredericq; **Grant sponsor:** Université de Liège (Fonds Spéciaux pour la Recherche - Crédits Sectoriels)
DOI: 10.1002/ijc.32247
History: Received 20 Aug 2018; Accepted 25 Feb 2019; Online 4 Mar 2019.
Correspondence to: Vincent Castronovo, Metastasis Research Laboratory, GIGA Cancer, University of Liege, Institute of Pathology B23, B-4000 Liège, Belgium, Tel: +32 4 3662480, Fax: +32 4 3662975, E-mail: vcastronovo@uliege.be

What's new?

While pancreatic ductal adenocarcinoma (PDAC) continues to have exceedingly low 5-year survival rates, there is hope that the discovery of reliable biomarkers and therapeutic targets can improve early diagnosis and treatment outcomes. To that end, the authors of this study identify the extracellular matrix protein transforming growth factor beta-induced (TGFBI) as a promising PDAC target. In PDAC patients, high TGFBI expression was associated with poor outcome. In PDAC cells, tumor aggressiveness was associated with greater TGFBI synthesis and secretion. Mechanistic analyses show that TGFBI activates FAK signaling *via* integrin αVβ5 binding, enhancing glycolysis and invasiveness in PDAC cells.

TGFBI, through integrin binding and interaction with ECM proteins, can promote the acquisition of a more invasive phenotype in several contexts.[12,13] In colorectal cancer, TGFBI overexpression was found to be responsible of cell extravasation and metastases dissemination.[14] On the other hand, studies have suggested opposite functions of TGFBI as a tumor suppressor.[15] This dual role of TGFBI in cancer may reflect the versatile behavior of its main modulator TGFβI.[16] Using a proteomic approach on resected PDAC tissues, we have previously identified TGFBI as a potential biomarker for targeted therapy.[17] In our study, TGFBI was expressed in PDAC lesions at a higher level than in nonneoplastic pancreas counterparts while it was barely detectable in healthy tissues. The role of TGFBI in PDAC is yet to be explored. In the present study, we demonstrate for the first time a pro-tumorigenic function for TGFBI produced by PDAC cancer cells. Through the binding to integrin αvβ5, TGFBI initiates focal adhesion kinase (FAK)-dependent signaling cascade that culminates into the upregulation of the transcription factor HIF-1α. Suppression of TGFBI expression impaired migratory and invasive abilities of PDAC cells. These effects were associated with a decrease of their glycolytic ability. In PDAC, impairment of this metabolic pathway is considered as a therapeutic approach with significant potential.[18] To our knowledge, this is the first time that TGFBI is described as a potential orchestrator of PDAC metabolism. In addition, TGFBI subcellular localization renders the protein easily accessible to specific monoclonal antibody targeting, opening opportunities for development of new treatments.

Material and Methods

Patient material

The use of human material for our study has been approved by the ethical committee of the University Hospital of Liege (#2016/270). Formalin-fixed paraffin-embedded PDAC samples were obtained from the institutional Biobank of the University Hospital of Liege, Belgium. According to Belgian law, informed consent was obtained using the opting-out procedure. Clinical characteristics of individual patients involved in the current study are outlined in Supporting Information Table S1.

Cell culture and reagents

All cells were recently purchased or authenticated by STR profiling performed by DSMZ institute (Braunschweig, Germany). Human PDAC cells HPAF-II (CRL-1997) were purchased from ATCC. BxPC-3 (CRL-1687) cells were a generous gift from Prof. Bikfalvi (Inserm U1029, Bordeaux, France). PANC-1 cells (CRL-1469) were a kind gift from Prof. Muller and Burtea (NMR Laboratory, University of Mons, Belgium). MiaPaCa-2 cells (ATCC CRL-1420) were a generous gift from Prof. De Wever (Laboratory of Experimental Cancer Research, University of Gent, Belgium). BxPC-3 cells were cultured in RPMI1640 medium supplemented with glucose (2.5 g/l), sodium pyruvate (1 mM) and Fetal Bovine Serum (FBS, 10%). PANC-1 cells were maintained in DMEM supplemented with FBS (10%), L-glutamine (2 mM) and nonessential amino acids. HPAF-II cells were cultured in MEM supplemented with FBS (10%), L-glutamine (2 mM), sodium pyruvate (1 mM) and nonessential amino acids. Miapaca-2 cells were cultured in DMEM supplemented with FBS (10%), L-glutamine (4 mM) and sodium pyruvate (1 mM). Cells were cultured in a 37°C incubator supplied with 5% CO_2. To assess the effect of exogenous TGFBI on AKT activation, 24 hr after seeding, PANC-1 cells (3.5×10^5) were starved in serum-free medium for 16 hr and then treated using 15 μg of recombinant human TGFBI protein (rhTGFBI, Targetome, Liège, Belgium). Cells were monthly checked for mycoplasma contamination and used between passage 1 and 10. All reagents were purchased from Sigma-Aldrich (Bornem, Belgium) unless mentioned otherwise. Antibodies were purchased from Targetome (Liège, Belgium): TGFBI (clone BY-4); Santa Cruz Laboratories (Santa Cruz, CA): HSC70 (sc-7298); BD Transduction Laboratories (Franklin Lakes, NJ): E-cadherin (#610181), integrin αv (CD51; #67141), FAK (#610088), HIF-1α (#610958); Sigma Life Sciences (Bornem, Belgium): vimentin (V6389); Cell Signaling (Danvers, MA): MEK2 (#9125), AKT (#9272), phospho-AKT (#4060), AMPK (#2795), phospho-AMPK (#2535), GLUT1 (#12939); Dako (Glostrup, Denmark): KI67 (M7240); and Merck-Millipore (Darmstadt, Germany): integrin $\alpha V\beta_5$ (clone P1F6, MAB1961), integrin $\alpha v\beta_3$ (MAB1976), phospho-FAK (MAB1144).

Immunohistochemistry

Tissue samples were sliced from paraffin blocks of PDAC (4 μm sections). Blocking of unspecific peroxidase activity was conducted for 30 min in H_2O_2 (3%) and methanol (90%). Sections were first subjected to antigen retrieval in citrate buffer (10 mM, pH 6, 95°C, 45 min) and then blocked in antibody diluent (Ventana Medical Systems, AZ). Tissues were immunostained using TGFBI antibody (dilution 1:500), overnight at 4°C. Sections were then washed in PBS and incubated for 30 min with secondary antibody solution (Nichirei Biosciences, Tokyo, Japan). The signal was revealed using 3,3′-diaminobenzidine tetrachlorhydrate

in H_2O_2 (5%). The tissues were counterstained with hematoxylin. Independent pathologist (EB) assessed immunohistochemistry (IHC) scoring. IHC were evaluated for the intensity of the staining using the following scale: 0 = no staining, 1 = weak, 2 = moderate and 3 = strong. The tissues were further evaluated for the extent of positivity using the scale: 1 = 0–33%, 2 = 33–66%, 3 = 66–100%. The values obtained by each of the two scales were multiplied to yield a composite value called IHC score.

Small interfering RNA transfection

Cells were transfected using small interfering RNA (siRNA, 40 nM) against TGFBI (On-Target Plus Human siTGFBI, L-019370-00-0005; Dharmacon) or irrelevant siRNA (On-Target Plus Non-targeting Pool, D-001810-10-05) using calcium phosphate as described previously.[19] Experiments were conducted 48 hr after transfection.

Short hairpin RNA transfection

Lentiviral vectors were generated as previously described,[20] and used to modify PANC-1 cells using irrelevant or TGFBI [CCGGCCACATCTTGAAGTCAGCTATCTCGAGTAGCTG ACTTAAGATGTGGTTTTTG] short hairpin RNA.

Lentiviral vectors generation and transduction

pLenti6-IRES-Luciferase plasmid was generated by cloning IRES (Internal Ribosome Entry Site) and Firefly luciferase sequences into a lentiviral plasmid using pLenti6/V5 Directional TOPO Cloning Kit (Invitrogen, Carlsbad, CA) in order to allow the expression of luciferase gene under the CMV promoter. The 2,052 bp of the *Homo sapiens* TGFBI cDNA (NM_000358.2) were synthetized (Genscript) and then cloned into pLenti6-IRES-Luciferase (EcoRV-NheI) to obtain the pLenti6-TGFBI-IRES-Luciferase plasmid for dual TGFBI and luciferase expression. Briefly, Lenti-X 293T cells (Clontech, Mountain View, CA) were co-transfected with a pSPAX2 and a VSV-G encoding vector. Viral supernatants were collected 48, 72 and 96 hr post transfection, filtrated (0.2 μm) and concentrated by ultracentrifugation. The lentiviral vectors were titrated with qPCR Lentivirus Titration Kit (ABM, LV900, Richmond, BC) and used to transduce MiaPaCa-2 cell line.

Migration assays

PANC-1 (2×10^5) and HPAF-II (2.5×10^5) cells were suspended in serum-free DMEM medium supplemented with BSA (0.1%) and penicillin/streptomycin (1%). Cells were seeded into the upper part of a Transwell filter (diameter 6.5 mm, pore size 8 μm). The lower compartment was filled with DMEM (PANC-1) and EMEM (HPAF-II) containing BSA (1%), penicillin/streptomycin (1%). Inserts were placed into a 37°C incubator supplied with CO_2 (5%). Twenty-four hours later, migrating cells were fixed and stained with Diff-Quick kit (Medion Diagnostics, Düdingen, Switzerland).

Invasion assays

PANC-1 cells (1.5×10^5) were prepared as above and seeded into the upper part of a Transwell filter (diameter 6.5 mm, pore size 8 μm) precoated with Matrigel (BD Biosciences). The lower compartment was filled as described above. Twenty-four hours later, invading cells were fixed and stained with Diff-Quick kit.

Migration and invasion quantification

Three representative pictures per each insert were taken and cells were counted using ImageJ.[21] Data were expressed as relative migration/invasion ability compared to control cells. Three biological replicates with two wells per condition were analyzed.

Cell proliferation

Assessment of cell proliferation was performed as previously described.[22] Briefly, 3×10^4 PANC-1 cells were seeded in complete medium 48 hr after transfection. DNA content was determined using Hoechst incorporation that is an indirect measure of cell number. Results shown are representative of three biological replicates.

Western blot

Total proteins were extracted in sodium dodecyl sulfate (SDS) (SDS, 1%) supplemented with protease and phosphatase inhibitors. Protein quantification was assessed using BCA Protein Assay (Thermo Scientific, Merelbeke, Belgium) according to the supplied protocol. Proteins (20 μg) were supplemented with Laemmli buffer and resolved on polyacrylamide (10%) denaturing gel then transferred onto nitrocellulose membranes and incubated overnight with primary antibody. Membranes were washed three times in TBS-tween then probed with corresponding secondary antibody conjugated to horseradish peroxidase for 1 hr at room temperature (RT). The immunoblots were revealed using chemiluminescent substrate (ECL, Thermo Scientific, Rockford, IL). Representative Western blots of three independent biological replicates are shown.

Adhesion assay

A low adherent 96 well-plate was coated with 20 μg/ml of purified human fibronectin (Calbiochem), laminin (Invitrogen), vitronectin (Chemicon) and a mix of the three compounds, overnight at 4°C. The remaining protein binding sites were blocked with TRIS-BSA (1%) for 30 min at RT. Meanwhile transiently transfected PANC-1 cells were trypsinized and resuspended in DMEM without serum supplemented with Insulin Transferrin Selenium (dilution: 1:100, Gibco) and BSA (0.1%). Cells (4×10^4) were seeded and let attaching for 1 hr. After a PBS wash, adherent cells were stained with crystal violet and quantified at 560 nm. Results represent the mean ± standard deviation of three biological experiments.

Dot blot assay

For the evaluation of ECM and TGFBI interactions, purified human recombinant fibronectin, laminin, vitronectin and a mix

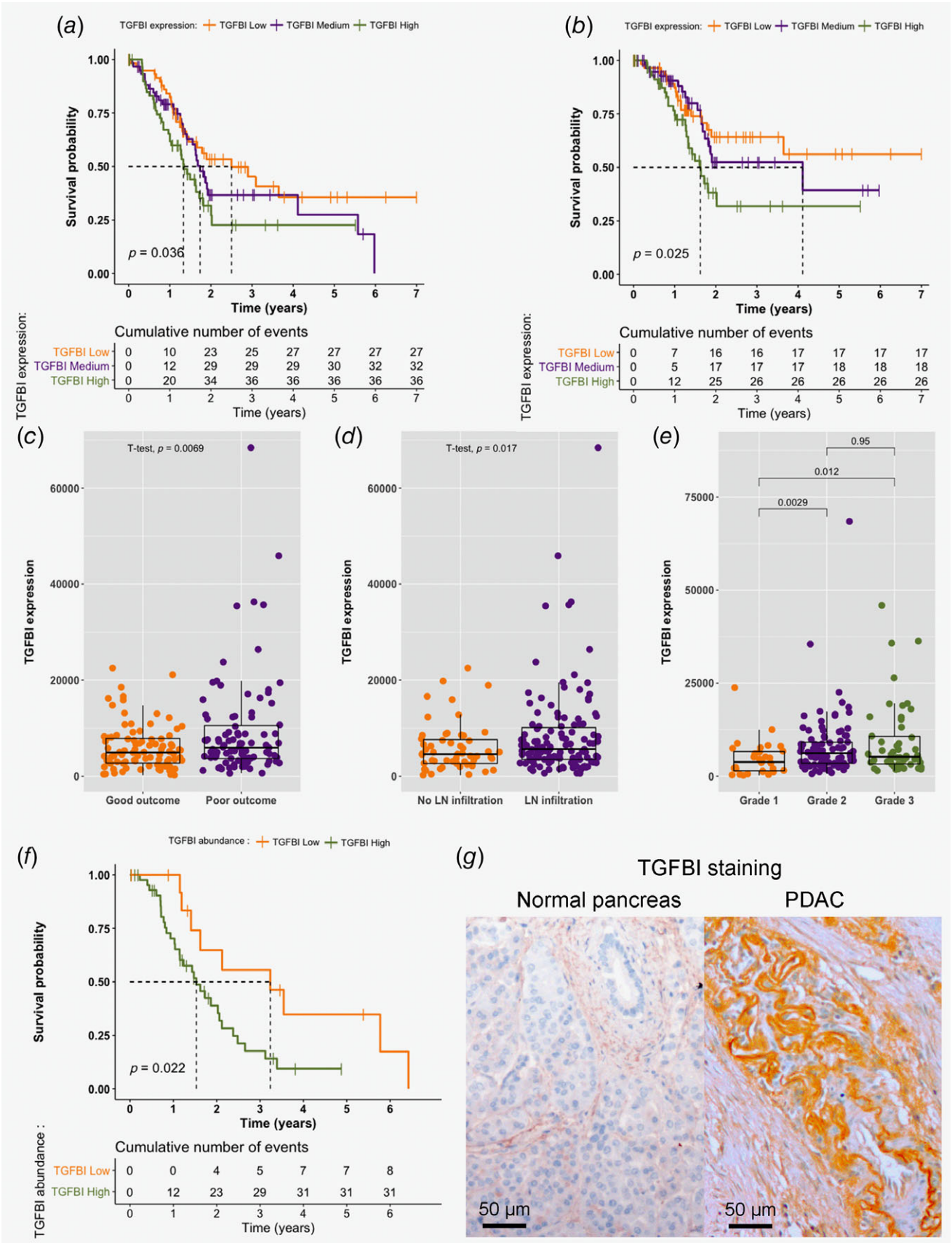

Figure 1. Legend on next page.

of three proteins were spotted onto a nitrocellulose membrane and dried under vacuum. ECM components were spotted at a concentration range varying from 0 to 40 μg/ml. The membrane was then blocked using TBS-Tween-BSA (5%) solution for 45 min and incubated overnight with rhTGFBI (5 μg/ml). After being washed three times in TBS-Tween solution, the membrane was incubated with TGFBI monoclonal antibody (dilution: 1:1000) for 2 hr at RT. Following washes in TBS-tween membrane was probed with anti-mouse secondary antibody 1 hr at RT. The binding of TGFBI to cell membrane proteins was evaluated by spotting increasing concentration of PANC-1 membrane-enriched proteins onto nitrocellulose membrane. After blocking as previously described, membrane was incubated with rhTGFBI (3 μg/ml) overnight at 4°C. Membrane was then probed with anti-TGFBI antibody. TGFBI and integrin interactions were evaluated by spotting on nitrocellulose membrane rhTGFBI in a concentration range varying from 2.5 to 20 μg/ml. After blocking, the membrane was incubated with PANC-1 membrane-enriched proteins (3 μg) overnight at 4°C. Membrane was incubated with antibodies directed against integrins αv, $\alpha v\beta_3$, or $\alpha v\beta_5$ for 2 hr at RT. After the incubation with the corresponding secondary HRP-conjugated antibodies, membranes were revealed using ECL.

Immunofluorescence

PANC-1, HPAF-II, BxPC-3 and MiaPaCa-2 cells (5×10^4) were seeded on glass coverslips in 24-well plates. Forty-eight hours after transient transfection cells were fixed/permeabilized with ice-cold methanol/acetone. After blocking (2% PBS-BSA for 30 min), slides were incubated overnight at 4°C with anti-HIF-1α, anti-TGFBI or anti-αvβ5 antibody diluted 1:50 in PBS-BSA (2%). After washing in PBS, slides were incubated with corresponding IgG-conjugated secondary antibodies (Life Technologies, dilution 1:1000) for 1 hr at RT. Nuclei were stained using DAPI. Coverslips were mounted on glass slides and observed using confocal microscope (Nikon A1R).

Extracellular flux analysis

Experiments were conducted in a Seahorse XFp extracellular flux analyzer (Agilent, Santa Clara, CA). Glycolysis stress test was performed on BxPC-3, MiaPaCa-2, PANC-1 and HPAF-II (1.5×10^4 cells/well) as previously described.[22] The readout of the assay was extracellular acidification rate (ECAR, mpH/min). All results were normalized according the Hoechst incorporation. Representative graphs of three independent experiments are shown.

Glucose uptake analysis

Experiments were conducted as described above (extracellular flux analysis). During the assay one single injection of glucose (25 mM) was performed and ECAR values were acquired for 80 min.

Nuclear magnetic resonance-based targeted metabolomics of cell medium

Targeted metabolomic analyses were conducted 48 hr after transfection. A volume of 300 μl of collected conditioned culture media were supplemented with 350 μl of deuterated phosphate buffer (pH 7.4), 50 μl of a 35 mM solution of maleic acid and 2 μl of TMSP. The solution was distributed into 5-mm tubes for NMR measurement. ^{1}H NMR spectra were acquired using a 1D NOESY sequence with presaturation and 32 transients and 4 dummy scans. The NMR spectra were recorded at 298 K on a spectrometer (Bruker) operating at 500.13 MHz for proton and equipped with a TCI cryoprobe (Bruker). Deuterium oxide (99.96%) and trimethylsilyl-3-propionic acid-*d*4 were purchased from Eurisotop (St-Aubin, France). Deuterated solvent was used as the internal lock. The data have been processed with Bruker TOSPIN 3.2 (Bruker) software with standard parameter set. Phase and baseline correction were performed manually over the entire range of the spectra and the δ scale was calibrated to 0 ppm using the internal standard trimethylsilyl-3-propionic acid-d4.

Lactate, glutamine and glucose concentrations were obtained by integrations of the lactate signal at 1.34 ppm, 2.45 ppm and 3.25 ppm, respectively, using maleic acid as internal standard (normalized to 2). The integral values were then corrected according to the number of cells.

Chorioallantoic membrane model

Tumor development on chorioallantoic membrane (CAM) was previously described.[23] On Embryonic Day 11, 100 μl of a suspension of 2×10^6 of BxPC-3 cells in culture medium mixed with Matrigel were deposited in the center of a plastic ring on the CAM. Tumors were collected on Embryonic Day 18. The tumors were fixed in paraformaldehyde (4%, 30 min) for histology analysis.

Statistical analysis

Kaplan-Meier survival curves were established based on The Cancer Genome Atlas (TCGA)-PAAD data imported using RTCGA packages.[24] Survival curves were compared using the log-rank test. Multivariate Cox regressions were performed

Figure 1. High TGFBI expression is correlated to poor patient outcome. TGFBI gene expression level in pancreatic cancer (PAAD) patients were retrieved from TCGA. Patient cohort (n = 183) was divided in tertiles for low, medium and high TGFBI expressing patients. Kaplan-Meier curves for patient (*a*) overall survival and (*b*) disease-specific survival are shown. Scatterplot were used for unveiling TGFBI expression difference between (*c*) patient outcome, (*d*) lymph-node infiltration status and (*e*) tumor histologic grade. Statistical analysis was performed using Student *T*-test or Wilcoxon's test according to group number. (*f*) Formalin-fixed paraffin-embedded sections of resected PDAC (n = 80) were immunostained with anti-TGFBI antibody. Quantitative evaluation of the staining was conducted as described under "Material and Methods" section. Kaplan-Meier curve was constructed to assess disease specific survival according to TGFBI abundance. (*g*) Representative pictures, taken at 400× magnification, of normal pancreas and PDAC immunostained for TGFBI.

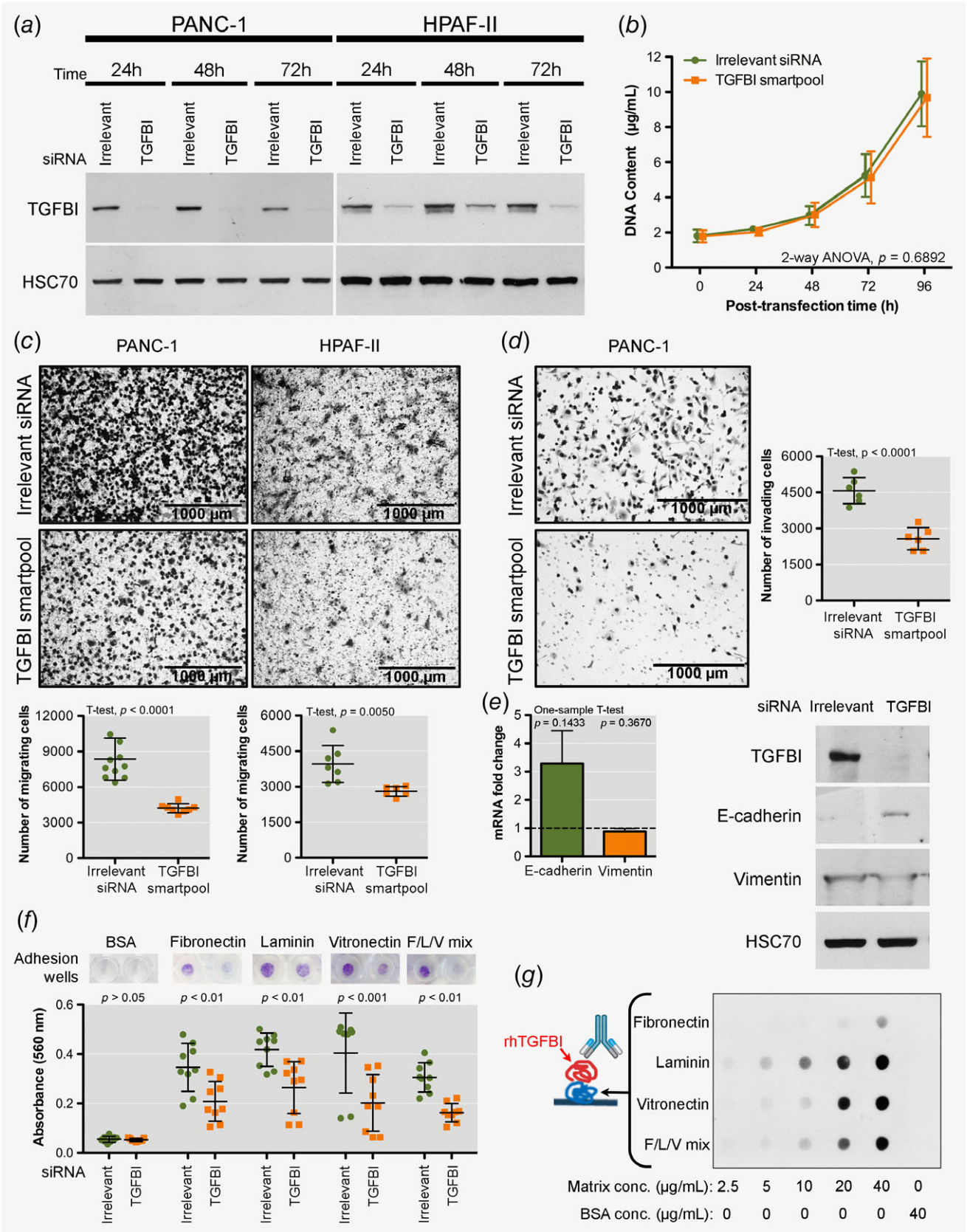

Figure 2. Legend on next page.

considering TGFBI as a discontinuous grouping variable (divided as tertiles) and followed by a log-rank test. All other results were reported as means with standard deviation. Two-sided statistical analyses were performed. Unless mentioned otherwise, group means were compared by unpaired Student's *T*-test or Bonferroni's pairwise comparison according to the group number. Welsch's correction was applied when homoscedasticity was suspected. All experiments were performed as several independent biological replicates. Statistics were performed using R v3.4.[25]

Results

High TGFBI expression negatively correlates with overall survival in PDAC patients

Tumor TGFBI gene expression levels were analyzed in 183 patients using the information available on TCGA dataset for pancreatic cancer (PAAD_TCGA). We first performed a survival analysis in accordance with TGFBI gene expression. Kaplan-Meier analysis indicated that high TGFBI gene expression was significantly associated with reduced patients overall survival (log-rank $p = 0.036$, Fig. 1*a*) and with reduced patient disease-specific survival (log-rank $p = 0.025$, Fig. 1*b*). The median overall survival times were 913 days, 634 days and 486 days for low, medium and high TGFBI expressing patients, respectively, while disease-specific survival times were 1,502 and 593 for medium and high TGFBI expression level, respectively. In this case, low TGFBI expressing patients never displayed less than 50% survivals. Patient cohort was further analyzed to unveil correlation between TGFBI expression and PDAC outcome. As shown in Figures 1*c*–1*e*, high TGFBI expression was significantly associated with poor patient outcome, increased lymph-node infiltration and higher tumor grades. In order to determine if TGFBI was an independent prognostic marker, we performed a multivariate Cox survival analysis with available clinical covariates (Supporting Information Table S2). The number of positive lymph nodes is the only significant factor ($p = 0.011$) in the prediction of the overall survival. TGFBI highest tertile showed a tendency ($p = 0.069$) in the prediction of the survival. Due to the high significance of the presence of positive lymph nodes to describe the survival, and in order to detect others valuable independent parameters, we decide to exclude the number of positive lymph nodes variable from the data before the analysis. In this condition, TGFBI highest tertile became the only significant factor ($p = 0.034$) with a hazard ratio of 2. These results indicate TGFBI as an independent predictor of survival.

Intrigued by these results, we next sought to verify whether the same tendency could be observed at protein level. Therefore, we have performed TGFBI immunostaining on resected PDAC from a cohort of 80 patients. Accordingly, disease-specific Kaplan-Meier analysis confirmed a worst outcome for patients having higher level of TGFBI (log-rank $p = 0.022$, Fig. 1*f*) with median survival times of 559 days versus 1,182 days for high and low TGFBI expressing patients, respectively. TGFBI is an ECM protein mainly secreted by fibroblasts.[26] Intriguingly, we observed that, in several lesions, cancer cells were also TGFBI positive (Fig. 1*g*, Supporting Information Fig. S1A) while normal pancreas tissues remained unstained. This observation led us to consult a gene expression dataset acquired for PDAC cells and accessible *via* cBioportal[27] which highlighted a heterogeneous expression of TGFBI within the searched PDAC cells (Supporting Information Fig. S1B). Using Western blot analysis, we demonstrated that PDAC cells expressed TGFBI in culture. TGFBI abundance was high in HPAF-II, BxPC-3 and PANC-1 cells and low in MiaPaCa-2 cells (Supporting Information Fig. S1C). Structurally TGFBI contains a N-terminal secretory signal peptide.[28] Thus, we have further verified its secretion by the selected cell lines. In accordance with previous results, we confirmed that aggressive PDAC cells secreted TGFBI more abundantly (Supporting Information Fig. S1D).

TGFBI depletion reduces migration and invasion of pancreatic cancer cells through alteration of cell–ECM interactions

To examine the potential role of TGFBI on PDAC cell phenotype, we silenced the expression of this protein using siRNA technique in PANC-1 and HPAF-II cells. Twenty-four to 72 hr after transfection, TGFBI levels were determined using Western blot analysis (Fig. 2*a*) showing an efficient TGFBI silencing during the experimental course. Cells were then assayed for their proliferative, migratory and invasive capacity. While PANC-1 did not demonstrate any alteration in proliferation upon TGFBI

Figure 2. TGFBI depletion reduces migration and invasion of pancreatic cancer cells through alteration of cell-ECM interaction. (*a*) Western blot analysis of PANC-1 and HPAF-II protein extracts 24–72 hr after TGFBI silencing. HSC70 is used as a loading control. (*b*) Assessment of cell proliferation through quantification of DNA content. Results are presented as mean with standard deviation ($n = 9$). (*c*) Analysis of PANC-1 and HPAF-II cell migration through Boyden chambers. A representative experiment out of three is shown. Scatterplot indicates the number of migrating cells/field ± standard deviation ($n > 6$). (*d*) Measurement of PANC-1 cell invasion through matrigel-coated Boyden chamber. A representative experiment out of three is shown. The scatterplot indicates the number of invading of cells/field ± standard deviation ($n = 6$). Both cell migration and invasion experiments were performed 48 hr after siRNA transient transfection. (*e*) On the left, E-cadherin and Vimentin mRNA expression fold change 48 hr after TGFBI silencing. Data are presented as a mean ± standard error ($n = 4$). Statistical analysis was performed by one-sample *T*-test. On the right, Western blot analysis of TGFBI, E-cadherin, vimentin proteins in PANC-1 cells 48 hr after TGFBI silencing. HSC70 is used as a loading control. (*f*) Adhesion assay of PANC-1 siRNA transfected cells to several ECM components. The absorbance values (560 nm) of crystal violet are shown as scatterplot. Data represent the mean ± standard deviation ($n = 9$). Statistical analysis was performed using 2-way ANOVA followed by Bonferroni's pairwise comparison. (*g*) rhTGFBI-ECM component interaction assay by adapted dot-blot assay. ECM components were spotted on nitrocellulose membrane further incubated with rhTGFBI. BSA was used as a negative control. TGFBI adhesion to ECM component was revealed by TGFBI antibody. [Color figure can be viewed at wileyonlinelibrary.com]

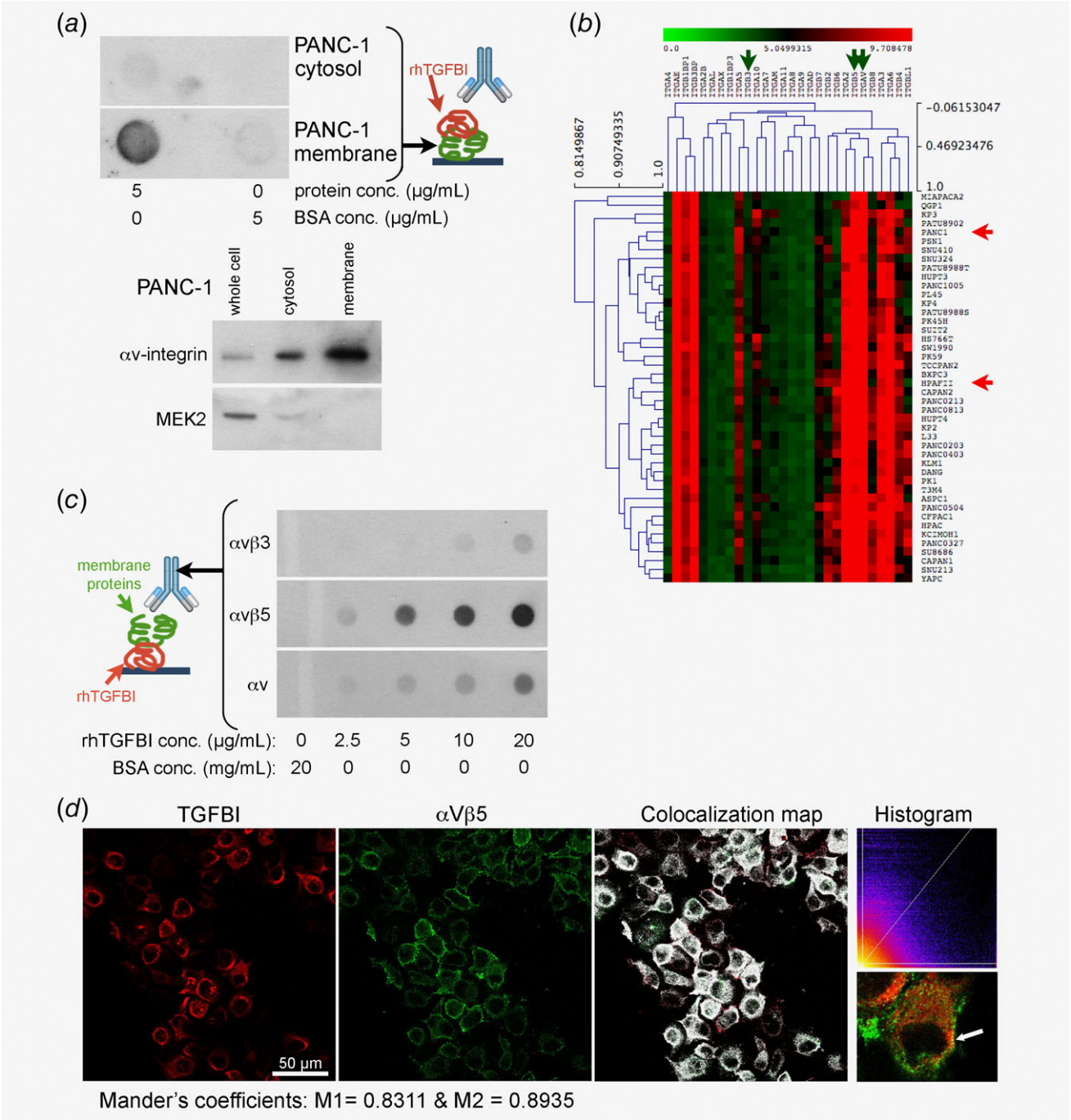

Figure 3. TGFBI binds to cell membrane protein integrin αv subunit. (*a*) In the upper panel, dot-blot analysis detecting TGFBI interaction with cytosolic and membrane-enriched PANC-1 proteins. BSA was used as a negative control. In the lower panel, Western blot analysis of αv integrin subunit and MEK2 was used as quality control of membrane and cytosolic extractions, respectively. (*b*) Heat-map analysis of integrin gene expression in 44 pancreatic cancer cell lines. Red arrows point to PANC-1 and HPAF-II cell lines. Green arrows point to integrin β3, β5 and αv subunits. (*c*) Dot-blot analysis revealing the interactions between TGFBI and αvβ3-, αvβ5-integrin heterodimers or αv integrin subunit. (*d*) Confocal images of αvβ5 integrin and TGFBI in PANC-1 cells. Colocalization map showed significant colocalization between αvβ5 integrin and TGFBI. Histogram showed the correlation between staining intensities in each channels.

silencing (Fig. 2*b*), we found a significant inhibition of cell migration in both PANC-1 and HPAF-II cell lines (Fig. 2*c*). Interestingly, TGFBI overexpression in the low expressing cell line MiaPaCa-2 increased cell migration by 50% (Supporting Information Fig. S2A). Furthermore, TGFBI-depleted PANC-1 cells exhibited significantly reduced invasive capabilities (Fig. 2*d*) suggesting a role for this protein in the acquisition of a migratory phenotype in PDAC. Migration and invasion are dynamic

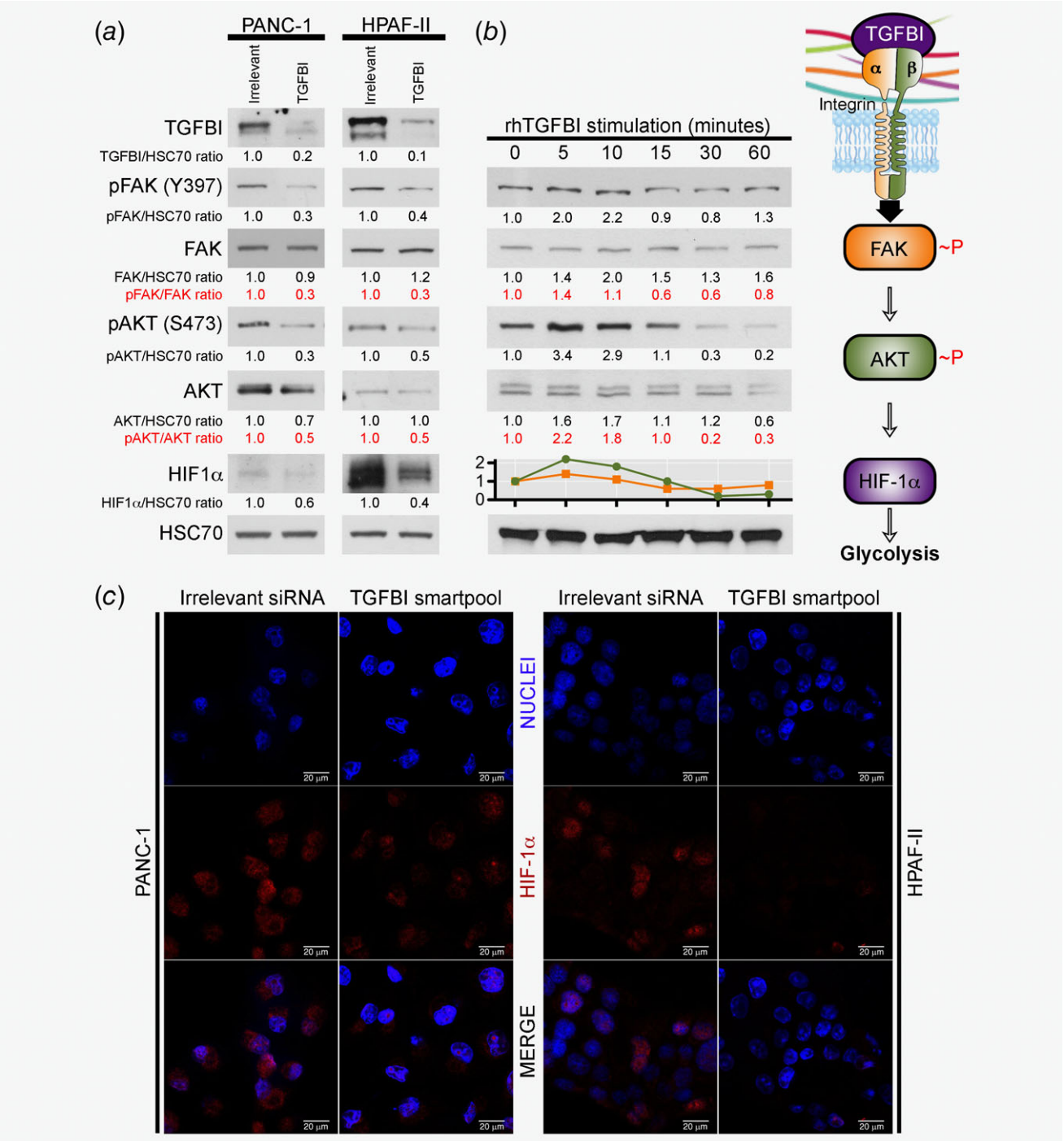

Figure 4. TGFBI activates FAK signaling cascade culminating with increased HIF-1α abundance. (*a*) Western blot analysis of TGFBI, pFAK (Y397), FAK, pAKT (S473), AKT and HIF-1α protein levels in PANC-1 and HPAF-II total cell extracts 48 hr after siRNA TGFBI transient transfection. HSC70 is used as a loading control. (*b*) Western blot analysis of FAK and AKT phosphorylation kinetic after rhTGFBI exposure. HSC70 is used as a loading control. Kinetic of phospho to nonphospho FAK (orange) and AKT (green) ratio was shown as a curve. (*c*) Immunofluorescence of HIF-1α in fixed and permeabilized PANC-1 and HPAF-II cells 48 hr after siRNA TGFBI transient transfection.

multistep processes where the initiating event is represented by the acquisition of spindle-shape morphology and interaction with ECM components. Cells in fact need to generate contacts with ECM where they create a permissive environment that can facilitate dissemination to distal sites.[29] In this context, we wanted to examine if the aforementioned effects on cell motility followed the outlined multisteps program. Forty-eight hours after transfection TGFBI-silenced PANC-1 cells evidenced a

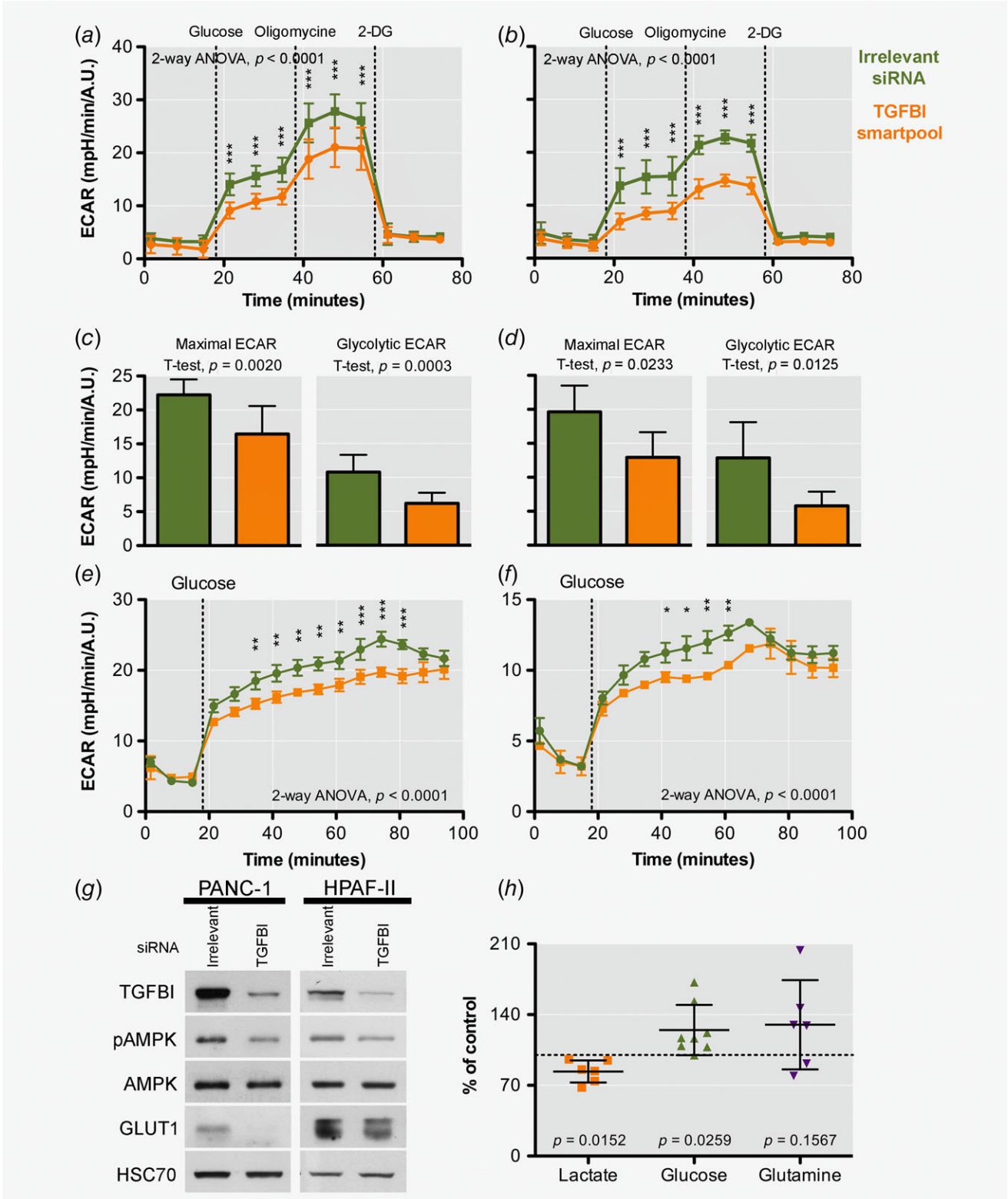

Figure 5. Legend on next page.

more epithelial-like morphology in comparison with the spindle-shaped control cells (Supporting Information Fig. S2B). Moreover E-cadherin was upregulated at both gene and protein levels in TGFBI-depleted cells (Fig. 2*e*). No significant changes could be observed for vimentin gene expression or protein abundance. A comparable transition was observed when a more

epithelial cell line (HPAF-II) was silenced for TGFBI (Supporting Information Fig. S2C). We further assessed the interactions between TGFBI and components of ECM. In the same experimental conditions, we verified the ability of PANC-1 cells to adhere to ECM components (fibronectin, laminin, vitronectin, or a mix of them). Our results demonstrated that lack of TGFBI significantly impaired the adhesive properties of PANC-1 cells toward all the tested ECM proteins (Fig. 2*f*). To further investigate the possibility that TGFBI can directly bind to ECM proteins, we have performed a custom dot-blot analysis where ECM components were immobilized onto a nitrocellulose membrane. Membrane was then incubated with rhTGFBI and revealed using anti-TGFBI antibody. We observed a dose-dependent interaction between TGFBI and ECM proteins (Fig. 2*g*) suggesting that the former could acts as linker protein, maybe to facilitate cell–matrix interactions.

TGFBI binds to integrin αvβ5, a cell membrane protein, and activates FAK signaling pathway

Intrigued by the previous results, we moved into the exploration of the molecular mechanism behind TGFBI actions in PDAC. Therefore, we have first assessed whether TGFBI would directly bind to cell-membrane proteins. Membrane-enriched PANC-1 proteins were spotted onto a nitrocellulose membrane that was further incubated with rhTGFBI and revealed using anti-TGFBI antibody. The dot-blot analysis clearly showed that TGFBI is able to bind preferentially proteins localized at cell surface (Fig. 3*a*). To identify the potential TGFBI binding partners, we consulted the STRING web-based tool,[30] which highlights protein–protein interactions. We found that integrin family was the preferential candidate to interact with TGFBI (Supporting Information Fig. S2D). Hence, a heat-map, showing integrin expression among PDAC cell lines, was constructed using gene expression data from cBioportal (Fig. 3*b*). We decided to concentrate our investigations on integrin-αv because it is ubiquitously expressed among the panel of all tested PDAC cells lines and studies had previously reported interactions between TGFBI and integrin αv subunit.[31] Using dot-blot technique, we demonstrated that TGFBI binds to integrin αv subunit and with more affinity to its heterodimer form αvβ5 (Fig. 3*c*). To further confirm the TGFBI-αvβ5 interaction, a colocalization analysis was performed by confocal microscopy followed by Mander's correlation analysis (Fig. 3*d*). Results indicated that 83% of the TGFBI staining coincides with the αvβ5 signal and that 89% of the αvβ5 localization coincides with the TGFBI one. The majority of this colocalization was at the vicinity of the plasma membrane. Integrins regulate cellular functions, including cell migration, through their coupling to cytoskeletal and signaling molecules that are colocalized with them in focal adhesions. FAK, a nonreceptor tyrosine kinase, is one of the most prominent signaling molecules among these proteins,[32] known to be stimulated by TGFBI in ovarian cancer cells.[33] Therefore, we have tested whether TGFBI silencing impacted on FAK phosphorylation in PDAC cell lines. Western blot analysis demonstrated that in both PANC-1 and HPAF-II cells, TGFBI silencing impaired FAK phosphorylation at tyrosine Y397 (Fig. 4*a*). In addition, we have observed a decreased phosphorylation of the downstream AKT protein (Fig. 4*a*). In support of these results, rhTGFBI treatment of PANC-1 cells demonstrated its ability to stimulate rapidly the FAK–AKT pathway (Fig. 4*b*). In order to show the importance of a TGFBI interaction with ECM in the activation of this pathway, cells were incubated with rhTGFBI with or without inhibiting RGD peptide (Supporting Information Fig. S3A). The RGD peptide reduced or delayed the activation of FAK and AKT, supporting the involvement of the TGFBI interaction with the ECM. Interestingly, the basal level of phosphorylated FAK in several PDAC cell lines correlated positively with the TGFBI secretion (Supporting Information Fig. S1C) and negatively with FAK inhibitor sensitivity revealed by its IC50 (Supporting Information Fig. S1E).

TGFBI modulates HIF-1α abundance and intensifies glycolysis

Recent reports pointed at FAK phosphorylation as an important regulator of glucose uptake and consumption.[34] In a previous publication Gan *et al.*, demonstrated that integrin–FAK signaling pathway resulted into the stabilization of hypoxia-inducible factor alpha (HIF-1α) that in turn favored increased glycolysis.[35] In light of our previous results, where TGFBI silencing impaired FAK phosphorylation and downstream AKT, we sought to investigate if this could have an impact on HIF-1α. Western blot analysis demonstrated a decrease of HIF-1α abundance in PDAC cells subjected to TGFBI silencing (Fig. 4*a*). Anti-HIF-1α immunofluorescence further confirmed our results in both

Figure 5. TGFBI enhances glycolysis in pancreatic cancer cell lines. Extracellular acidification rate (ECAR) in (*a*) PANC-1 and (*b*) HPAF-II cells depleted of TGFBI in response to successive injection of glucose (10 mM), oligomycin (1 μM) and 2-deoxyglucose (2DG, 50 mM). Results were normalized according to cell number by Hoechst incorporation (arbitrary unit, A.U.). Results represent the mean ± standard deviation ($n = 3$). Two-way ANOVA followed by Bonferroni's pairwise comparison was used for statistical evaluations (***$p < 0.001$). Basal and maximal glycolytic capacities were determined in the same experimental setting for PANC-1 (*c*) and HPAF-II (*d*). Statistic significance was determined using Student *T*-test analysis. (*e*–*f*) ECAR measurements indicating the kinetic of glucose consumption in (*e*) PANC-1 and (*f*) HPAF-II cell lines upon TGFBI silencing. Measurements were carried out for 80 min after single injection of glucose (25 mM). Results were normalized according to cell number by Hoechst incorporation (arbitrary unit, A.U.). Results represent the mean ± standard deviation ($n = 3$). Two-way ANOVA followed by Bonferroni's pairwise comparison was used for statistical evaluations (*$p < 0.05$, **$p < 0.01$, ***$p < 0.001$). (*g*) Western blot analysis of pAMPK, AMPK and GLUT1 in PANC-1 and HPAF-II cells silenced for TGFBI. HSC70 is used as a loading control. (*h*) NMR metabolomic analysis of cell culture-conditioned media collected 48 hr after siRNA transfection in PANC-1 cell line. Data were normalized to the cell number at the moment of media collection. Lactate, glucose and glutamine dosage are reported as relative % of control condition. Results shown the mean ± standard deviation ($n > 6$). Statistical analysis was performed by one-sample *T*-test.

PANC-1 and HPAF-II cell lines (Fig. 4*c*). As supporting information, HIF-1α nuclear localization was more frequent in high secreting TGFBI cell lines (BxPC-3 and HPAF-II) than in low secreting cell lines (PANC-1 and MiaPaCa-2) (Supporting Information Fig. S3B). Considering the role of HIF-1α as a central regulator of glycolysis, we have hypothesized that PDAC cells lacking TGFBI could be exposed to modifications of this metabolic way. To test this hypothesis, we measured the ECAR in PANC-1 and HPAF-II siRNA-transfected cells after successive addition of glucose, oligomycin and 2-deoxyglucose. The results demonstrated a significant impairment of ECAR in TGFBI-depleted cells (Figs. 5*a* and 5*b*). Moreover, we observed that both maximal and basal glycolytic ECAR were significantly reduced in silenced cells than in control conditions (Figs. 5*c* and 5*d*). Similarly, basal glycolytic ECAR and spare ECAR capacity of BxPC-3, HPAF-II, PANC-1 and MiaPaCa-2 cell lines were correlated to the level of secreted TGFBI (Supporting Information Fig. S3C). Moreover, TGFBI overexpression in the low expressing MiaPaCa-2 cell line increased significantly the kinetic ECAR (Supporting Information Fig. S4A) leading to an unchanged basal ECAR (Supporting Information Fig. 4*b*) but to an enhanced maximal ECAR (Supporting Information Fig. 4*c*) and spare capacity (Supporting Information Fig. S4D). High glycolytic rates are sustained by increased nutrients consumption. Cellular energy homeostasis is fine tuned by nutrient sensors such as AMPK whose phosphorylation occurs in response to energetic stress. Forty-eight hours after transfection, we have noticed a higher exhaustion of cell culture medium marked by increased acidification levels in control condition (data not shown). This situation favored activation of AMPK as demonstrated through higher accumulation of pAMPK in control than in TGFBI-depleted PANC-1 and HPAF-II cells (Fig. 5*g*). We have further evaluated the kinetic of glucose uptake and its consumption by ECAR measurements after a single injection of glucose. As demonstrated in Figure 5*e* for PANC-1 and Figure 5*f* for HPAF-II cells depleted of TGFBI consumed glucose at lower rate than control cells. In line with this result, we assisted to a downregulation of GLUT1, the main transporter of glucose, in PDAC cell lines upon TGFBI silencing (Fig. 5*g*). We next proceeded with a metabolomic analysis of cell culture media collected 48 hr after TGFBI siRNA transient transfection. ^{1}H-NMR quantified spectra revealed a significant decrease of lactate secretion alongside with glucose accumulation in cell media of TGFBI-silenced PANC-1 by comparison with control cells. A similar, but not significant, accumulation of glutamine was found in culture media after TGFBI silencing (Fig. 5*h*).

TGFBI depletion impairs tumor growth

Our next question was to investigate if loss of TGFBI in PDAC cells had an effect on tumor growth *in vivo*. Thus, we implanted onto the CAM of chicken embryos BxPC-3 cells, a model that mimics pancreas cancer development,[23] and we evaluated tumor growth in presence or absence of TGFBI. The efficiency of TGFBI siRNA transfection was evaluated and was sustained during a 6-day period (Fig. 6*a*). On Day 7 after cell implantation, tumors were excised from the CAM and volumes were calculated. TGFBI depletion significantly reduced BxPC-3 tumor growth as demonstrated in Figures 6*b* and 6*c*. Ki67-positive cells number was moderately reduced by TGFBI suppression (Figs. 6*d* and 6*e*).

Discussion

Cumulative pieces of evidence point at TGFBI as a promoter of local tumor growth and metastatic progression. More specifically, TGFBI expression was linked to the acquisition of a more aggressive phenotype in colon[14] and pancreas cancer.[36] In prostate cancer models, TGFBI silencing reduced local tumor growth and metastatic dissemination to distal organs extending the survival of tumor-bearing mice.[37] A similar behavior was described also for gastrointestinal cancer[38] and glioma.[39] However, the role of TGFBI signaling in solid tumors appears versatile since it can exhibit antitumor activities depending on disease and stage.[15] As we have demonstrated a significant link between TGFBI abundance and patient low survival, our findings are supportive of a tumor promoter role for TGFBI in PDAC. Such correlation was suggested by TGFBI levels measured in patients sera.[38] In line with the prometastatic role envisioned for TGFBI we showed, *in vitro,* that it enhanced migration and invasion of PDAC cells. Although some studies have attempted to explore the mechanism underlying TGFBI tumor-promoting role in cancer, up-to-date little is known concerning PDAC (While we were preparing the revised version of this manuscript, Goehrig and colleagues reported a pro-tumorigenic function for TGFBI in PDAC. http://dx.doi.org/10.1136/gutjnl-2018-317570). In the present study, we found that TGFBI is able to directly interact with ECM proteins conferring to PDAC cells increased adhesive properties, essential for the earlier steps of migration. We next demonstrated that TGFBI is able to bind to integrin proteins. This role was described in keratinocytes with α3β1 integrin where it allowed their spreading.[12] The existence of a TGFBI–ECM–integrin axis in PDAC represents a potential opportunity for development of new therapeutic strategies.[40] It is, indeed, widely recognized that integrin-mediated tumor cell interactions with the ECM have a crucial role in driving the malignant phenotype of solid tumors and in conferring intrinsic chemotherapeutic resistance.[41] This is particularly true for malignancy like PDAC characterized by prominent hyperplasia of the stromal surrounding tumor cells. It is worth noting that TGFBI is ubiquitously expressed in both epithelial and stromal tumor compartments where it may contribute to enforce the ECM deposition. Therefore, TGFBI targeting could offer a double approach to limit PDAC dissemination. The use of a TGFBI knock-out mice model would allow to ultimately prove this hypothesis.

PDAC are highly dependent on KRAS mutations, occurring in most of the patients, for several steps of cancer progression including initiation, metabolic adaptation, maintenance and dissemination.[42–44] In PDAC, the expression of this oncogene is associated with a reduced efficacy of therapeutic agents[45,46] and

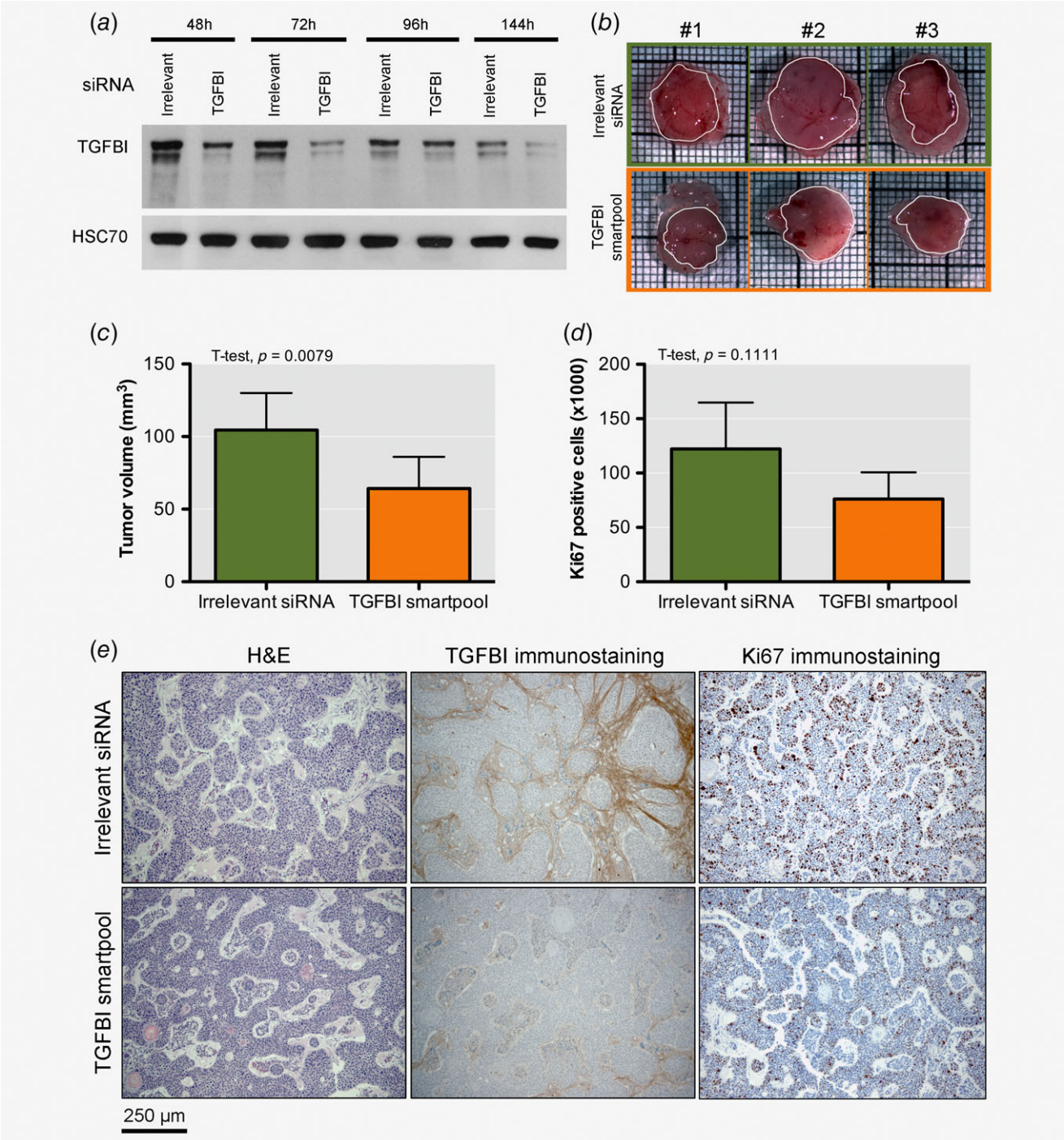

Figure 6. TGFBI depletion impairs tumor growth in CAM model. (*a*) TGFBI Western blot analysis to assess the efficiency of the transfection for full duration of experimental setting. HSC70 is used as a loading control. (*b*) Representative pictures of excised tumor 7 days post implantation. Tumor boundaries are shown in white. (*c*) Tumor volumes were measured using caliper and average volumes are reported as mean ± standard deviation ($n = 6$ for irrelevant siRNA and $n = 8$ for TGFBI smartpool). (*d*) Quantification of Ki67 positive cells in CAM tumors. (*e*) Hematoxylin-Eosin (H&E), TGFBI and Ki67 immunostaining of representative CAM formalin-fixed paraffin-embedded tissues. [Color figure can be viewed at wileyonlinelibrary.com]

to a metabolic shift toward anabolic metabolism.[47] The latter further contributes to acquired chemoresistance.[48] As such, alteration of this metabolic way is taken into account for therapeutic purposes. To our knowledge, our data represent the first evidence of a central role for TGFBI as an orchestrator of the PDAC glycolysis through modulation of FAK–AKT–HIF-1α

axis. FAK-mediated glycolysis regulation has been previously observed in PDAC.[34] In our cell models, TGFBI depletion impaired FAK phosphorylation and downstream AKT leading to a decreased abundance of HIF-1α protein. Rapid intake of glucose and augmented levels of GLUT1 were observed in TGFBI-expressing PDAC cells. A recent study exploring the metabolic differences between primary PDAC and matched metastasis demonstrated in the latter a robust overexpression of several glycolytic genes, mainly GLUT1.[49] Interestingly, hexokinase-2 was shown as necessary for invasion in PDAC cell lines,[50] underlying the importance of impairing glycolysis in PDAC progression. Because, TGFBI was initially identified as an accessible tumor-associated protein,[17] our present work pointed out this ECM tumor-associated protein, barely or not expressed in normal tissue, as a potential target for PDAC therapy.

Acknowledgements

Authors acknowledge Dr Chantal Humblet and Mrs Alice Marquet (GIGA-histology platform, ULg), Drs Sandra Ormenese and Jean-Jacques Goval (GIGA-imaging platform, ULg), Dr Emmanuel Di Valentin (GIGA-viral vector platform, ULg), Mrs. Naima Maloujahmoum (Metastasis Research Laboratory), Mr. Ferman Agirman (Metastasis Research Laboratory), Mr. Patrick Roncarati (Laboratory of Experimental Pathology) for their respective experimental support. We are also thankful to the institutional Biobank of the University Hospital Liege for providing patient material. The results shown in this work are in part based upon data generated by the TCGA Research Network: http://cancergenome.nih.gov/. Akeila Bellahcène and Pascal De Tullio are Research Directors (FNRS). Dr Brunella Costanza and Mrs Justine Bellier are supported by a FNRS Télévie grant. Dr Turtoi is a senior research fellow of the French National Institute of Health and Medical Research (INSERM) and is supported by LabEx MabImprove Starting Grant. This research was supported by the Léon Fredericq Fondation and by the University of Liège (Fonds Spéciaux pour la Recherche – Crédits Sectoriels). The sponsors have no other roles in the study.

Author contributions

BC, GR, ATi, JL and JB performed experiments and acquired data. BC, OP, PD, VC and AB analyzed data. JL and PdD performed and analyzed NMR. EB reviewed and scored immunostained sections. PdD and PD gave access to needed equipment and expertise. OP and VC conceived and designed experiments. OP performed statistical analysis. BC and OP wrote the manuscript. AT corrected and criticized the manuscript. All authors proofread the manuscript, contributed to the redaction of their specific part and approved the final version.

References

1. Siegel RL, Miller KD, Jemal A. Cancer statistics, 2016. *CA Cancer J Clin* 2016;66:7–30.
2. Rahib L, Smith BD, Aizenberg R, et al. Projecting cancer incidence and deaths to 2030: the unexpected burden of thyroid, liver, and pancreas cancers in the United States. *Cancer Res* 2014;74:2913–21.
3. Rhim AD, Mirek ET, Aiello NM, et al. EMT and dissemination precede pancreatic tumor formation. *Cell* 2012;148:349–61.
4. Chan A, Diamandis EP, Blasutig IM. Strategies for discovering novel pancreatic cancer biomarkers. *J Proteomics* 2013;81:126–34.
5. Longo V, Brunetti O, Gnoni A, et al. Angiogenesis in pancreatic ductal adenocarcinoma: a controversial issue. *Oncotarget* 2016;7:58649–58.
6. Raphael BJ, Hruban RH, Aguirre AJ, et al. Integrated genomic characterization of pancreatic ductal adenocarcinoma. *Cancer Cell* 2017;32:185–203. e13.
7. Hardie R-A, van Dam E, Cowley M, et al. Mitochondrial mutations and metabolic adaptation in pancreatic cancer. *Cancer Metab* 2017;5:2.
8. Pandol S, Edderkaoui M, Gukovsky I, et al. Desmoplasia of pancreatic ductal adenocarcinoma. *Clin Gastroenterol Hepatol* 2009;7:S44–7.
9. Bonnans C, Chou J, Werb Z. Remodelling the extracellular matrix in development and disease. *Nat Rev Mol Cell Biol* 2014;15:786–801.
10. Hwang RF, Moore T, Arumugam T, et al. Cancer-associated stromal fibroblasts promote pancreatic tumor progression. *Cancer Res* 2008;68:918–26.
11. Grzesiak JJ, Ho JC, Moossa AR, et al. The integrin-extracellular matrix Axis in pancreatic Cancer. *Pancreas* 2007;35:293–301.
12. Bae J-S, Lee S-H, Kim J-E, et al. Betaig-h3 supports keratinocyte adhesion, migration, and proliferation through alpha3beta1 integrin. *Biochem Biophys Res Commun* 2002;294:940–8.
13. Kim M-O, Yun S-J, Kim I-S, et al. Transforming growth factor-β-inducible gene-h3 (βig-h3) promotes cell adhesion of human astrocytoma cells in vitro: implication of α6β4 integrin. *Neurosci Lett* 2003;336:93–6.
14. Ma C, Rong Y, Radiloff DR, et al. Extracellular matrix protein betaig-h3/TGFBI promotes metastasis of colon cancer by enhancing cell extravasation. *Genes Dev* 2008;22:308–21.
15. Li B, Wen G, Zhao Y, et al. The role of TGFBI in mesothelioma and breast cancer: association with tumor suppression. *BMC Cancer* 2012;12:239.
16. Shen W, Tao G-Q, Zhang Y, et al. TGF-ß in pancreatic cancer initiation and progression: two sides of the same coin. *Cell Biosci* 2017;7:39.
17. Turtoi A, Musmeci D, Wang Y, et al. Identification of novel accessible proteins bearing diagnostic and therapeutic potential in human pancreatic ductal adenocarcinoma. *J Proteome Res* 2011;10:4302–13.
18. Halbrook CJ, Lyssiotis CA. Employing metabolism to improve the diagnosis and treatment of pancreatic cancer. *Cancer Cell* 2017;31:5–19.
19. Peixoto P, Castronovo V, Matheus N, et al. HDAC5 is required for maintenance of pericentric heterochromatin, and controls cell-cycle progression and survival of human cancer cells. *Cell Death Differ* 2012;19:1239–52.
20. Nokin M-J, Durieux F, Peixoto P, et al. Methylglyoxal, a glycolysis side-product, induces Hsp90 glycation and YAP-mediated tumor growth and metastasis. *Elife* 2016;5:260.
21. Schneider CA, Rasband WS, Eliceiri KW. NIH image to ImageJ: 25 years of image analysis. *Nat Methods* 2012;9:671–5.
22. Rademaker G, Hennequière V, Brohée L, et al. Myoferlin controls mitochondrial structure and activity in pancreatic ductal adenocarcinoma, and affects tumor aggressiveness. *Oncogene* 2018;66:1–15.
23. Peulen O, Gonzalez A, Peixoto P, et al. The anti-tumor effect of HDAC inhibition in a human pancreas cancer model is significantly improved by the simultaneous inhibition of cyclooxygenase 2. *PLoS One* 2013;8:e75102.
24. Kosinski M, Biecek P. RTCGA: The cancer genome atlas data integration. Available from: https://rtcga.github.io/RTCGA
25. R Development Core Team. *R: A language and environment for statistical computing*. Vienna: R Foundation for Statistical Computing, 2008 Available from: http://www.R-project.org.
26. Thapa N, Lee B-H, Kim I-S. TGFBIp/betaig-h3 protein: a versatile matrix molecule induced by TGF-beta. *Int J Biochem Cell Biol* 2007;39:2183–94.
27. Gao J, Aksoy BA, Dogrusoz U, et al. Integrative analysis of complex Cancer genomics and clinical profiles using the cBioPortal. *Sci Signal* 2013;6:pl1–1.
28. Skonier J, Neubauer M, Madisen L, et al. cDNA cloning and sequence analysis of beta ig-h3, a novel gene induced in a human adenocarcinoma cell line after treatment with transforming growth factor-beta. *DNA Cell Biol* 1992;11:511–22.
29. Lambert AW, Pattabiraman DR, Weinberg RA. Emerging biological principles of metastasis. *Cell* 2017;168:670–91.
30. Szklarczyk D, Franceschini A, Wyder S, et al. STRING v10: protein–protein interaction networks, integrated over the tree of life. *Nucleic Acids Res* 2014;43:D447–52.
31. Nummela P, Lammi J, Soikkeli J, et al. Transforming growth factor beta-induced (TGFBI) is an anti-adhesive protein regulating the invasive growth of melanoma cells. *Am J Pathol* 2012;180:1663–74.
32. Zhao X, Guan J-L. Focal adhesion kinase and its signaling pathways in cell migration and angiogenesis. *Adv Drug Deliv Rev* 2011;63:610–5.

33. Ahmed AA, Mills AD, Ibrahim AEK, et al. The extracellular matrix protein TGFBI induces microtubule stabilization and sensitizes ovarian cancers to paclitaxel. *Cancer Cell* 2007;12:514–27.
34. Zhang J, Gao Q, Zhou Y, et al. Focal adhesion kinase-promoted tumor glucose metabolism is associated with a shift of mitochondrial respiration to glycolysis. *Oncogene* 2016;35:1926–42.
35. Gan L, Meng J, Xu M, et al. Extracellular matrix protein 1 promotes cell metastasis and glucose metabolism by inducing integrin β4/FAK/-SOX2/HIF-1α signaling pathway in gastric cancer. *Oncogene* 2018;37:744–55.
36. Balasenthil S, Chen N, Lott ST, et al. A migration signature and plasma biomarker panel for pancreatic adenocarcinoma. *Cancer Prev Res (Phila)* 2011;4:137–49.
37. Chen WY, Tsai YC, Yeh HL, et al. Loss of SPDEF and gain of TGFBI activity after androgen deprivation therapy promote EMT and bone metastasis of prostate cancer. *Sci Signal* 2017;10:eaam6826.
38. Han B, Cai H, Chen Y, et al. The role of TGFBI (βig-H3) in gastrointestinal tract tumorigenesis. *Mol Cancer* 2015;14:64.
39. Pan Y-B, Zhang C-H, Wang S-Q, et al. Transforming growth factor beta induced (TGFBI) is a potential signature gene for mesenchymal subtype high-grade glioma. *J Neurooncol* 2018;137:395–407.
40. Li X, Ma Q, Xu Q, et al. Targeting the cancer-stroma interaction: a potential approach for pancreatic cancer treatment. *Curr Pharm Des* 2012;18:2404–15.
41. Liang C, Shi S, Meng Q, et al. Complex roles of the stroma in the intrinsic resistance to gemcitabine in pancreatic cancer: where we are and where we are going. *Exp Mol Med* 2017;49:e406.
42. Ying H, Kimmelman AC, Lyssiotis CA, et al. Oncogenic Kras maintains pancreatic tumors through regulation of anabolic glucose metabolism. *Cell* 2012;149:656–70.
43. Collins MA, Brisset J-C, Zhang Y, et al. Metastatic pancreatic cancer is dependent on oncogenic Kras in mice. *PLoS One* 2012;7:e49707.
44. Collins MA, Bednar F, Zhang Y, et al. Oncogenic Kras is required for both the initiation and maintenance of pancreatic cancer in mice. *J Clin Invest* 2012;122:639–53.
45. Réjiba S, Wack S, Aprahamian M, et al. K-ras oncogene silencing strategy reduces tumor growth and enhances gemcitabine chemotherapy efficacy for pancreatic cancer treatment. *Cancer Sci* 2007;98:1128–36.
46. Yang K, Li Y, Lian G, et al. KRAS promotes tumor metastasis and chemoresistance by repressing RKIP via the MAPK-ERK pathway in pancreatic cancer. *Int J Cancer* 2018;142:2323–34.
47. Kimmelman AC. Metabolic dependencies in RAS-driven cancers. *Clin Cancer Res* 2015;21:1828–34.
48. Grasso C, Jansen G, Giovannetti E. Drug resistance in pancreatic cancer: impact of altered energy metabolism. *Crit Rev Oncol Hemat* 2017;114:139–52.
49. Chaika NV, Yu F, Purohit V, et al. Differential expression of metabolic genes in tumor and stromal components of primary and metastatic loci in pancreatic adenocarcinoma. *PLoS One* 2012;7:e32996.
50. Anderson M, Marayati R, Moffitt R, et al. Hexokinase 2 promotes tumor growth and metastasis by regulating lactate production in pancreatic cancer. *Oncotarget* 2016;8:56081–94.